Check for updates

Attack of hydroxyl radicals to α-methyl-styrene sulfonate polymers and cerium-mediated repair *via* radical cations†

Tom M. Nolte, [iD] ‡*[ab] Thomas Nauser [iD] [b] and Lorenz Gubler [iD] [a]

Both synthetic polymers (membranes, coatings, packaging) and natural polymers (DNA, proteins) are subject to radical-initiated degradation. In order to mitigate the deterioration of the polymer properties, antioxidant strategies need to be devised. We studied the reactions of poly(α-methylstyrene sulfonate), a model compound for fuel cell membrane materials, with different degrees of polymerization with OH• radicals as well as subsequent reactions. We observed the resulting OH•-adducts to react with oxygen and eliminate H_2O, the relative likelihood of which is determined by pH and molecular weight. The resulting radical cations can be reduced back to the parent molecule by cerium(III). This 'repair' reaction is also dependent on molecular weight likely because of intramolecular stabilization. The results from this study provide a starting point for the development of new hydrocarbon-based ionomer materials for fuel cells that are more resistant to radical induced degradation through the detoxification of intermediates *via* damage transfer and repair pathways. Furthermore, a more fundamental understanding of the mechanisms behind conventional antioxidants in medicine, such as ceria nanoparticles, is achieved.
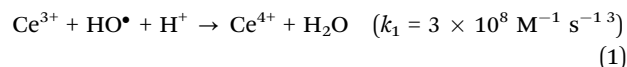
Introduction

Oxidative stress is a critical lifetime-limiting factor for sulfonated polyaromatic proton exchange membranes (PEMs) in the polymer electrolyte fuel cell (PEFC). These ionomers are of interest to replace the widely used perfluoroalkylsulfonic acid (PFSA) membranes, owing to their much lower gas permeability, higher glass transition temperature, and potentially lower cost.[1] Oxidative stress is created by the presence of radical species, such as HO•, H• and HOO•, which are formed during the operation of the fuel cell in the presence of H_2, O_2, and the noble metal catalyst.[2]

The hydroxyl radical (HO•) can be particularly detrimental to the polymer as it initiates degradation. HO• reacts with aromatic compounds with typical rate constants in the range of the diffusion limit of 10^9–10^{10} M^{-1} s^{-1}.[3,4] However, the nature of follow-up reactions, intermediates and the associated kinetics are rarely considered. The final result of HO• attack may be chain oxidation (*e.g.*, hydroxylation), crosslinking, or

chain fragmentation.[5] These different mechanisms of polymer aging depend on the chemistry of the polymer. Thus, strategies to prevent aging ought to take these pathways into account (Fig. 1). For example, 'repairing' intermediates formed upon radical attack may be accomplished with suitable additives, *i.e.*, antioxidants (*e.g.* in Fig. 1, reaction 11).[6]

There is an analogy to oxidative stress in living cells: here, it is the characteristic of imbalance between reactive oxygen species (ROS) generation and an organism's endogenous defenses. OH• is generated from 'leakage' of electrons along the cellular electron transport chain, and can react with cell constituents (DNA, proteins). As a consequence, oxidative stress is the basis of many serious diseases such as cancer. Nature has its way of detoxifying radicals, *i.e.*, using vitamins and enzymes. When these endogenous mechanisms to combat oxidative stress fall short, we can consider treatment *via* synthetic alternatives. Ceria nanoparticles (CNPs) are promising inorganic antioxidants for many biomedical applications. CNPs have demonstrated antioxidant enzyme-mimetic activity, as well as the capacity to scavenge a variety of ROS in both cell and animal models. Concomitantly, a reduction in DNA damage (*e.g.* in lung cells) has been observed.[7] Cerium ions or ceria particles are also used to mitigate degradation in PFSA-type fuel cell membranes[8] *via* direct scavenging of OH•, and potentially H•:[9,10]

$$Ce^{3+} + HO• + H^+ \rightarrow Ce^{4+} + H_2O \quad (k_1 = 3 \times 10^8 \ M^{-1} \ s^{-1} \ [3])$$

(1)

[a] *Electrochemistry Laboratory, Paul Scherrer Institut, 5232 Villigen PSI, Switzerland. E-mail: t.nolte@science.ru.nl*

[b] *Eidgenössische Technische Hochschule (ETH) Zurich, Laboratory of Inorganic Chemistry, Vladimir-Prelog-Weg 1, 8093 Zurich, Switzerland*

‡ Current address: Department of Environmental Science, Institute for Water and Wetland Research, Radboud University Nijmegen, 6500 GL Nijmegen, The Netherlands.
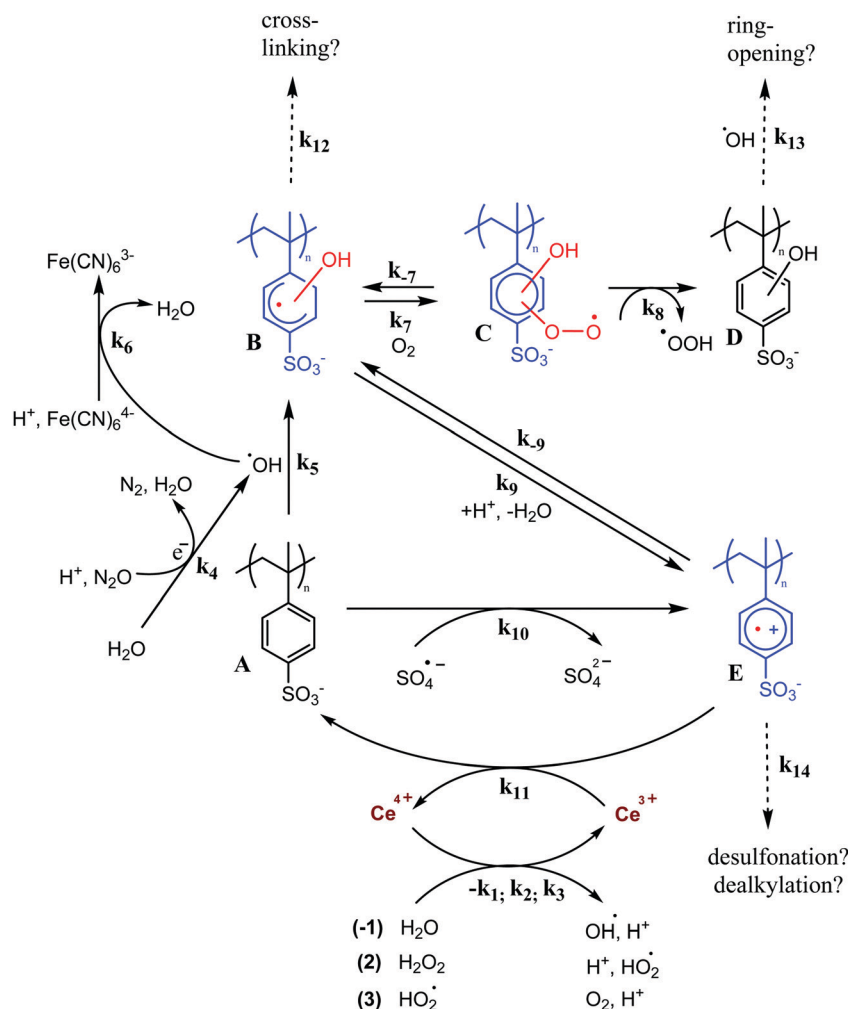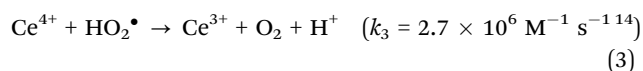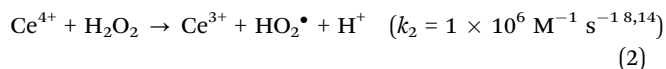
Fig. 1 Reaction pathways considered in this study. Reaction between the PAMSS polymer/oligomer (compound **A**) with OH$^\bullet$ (reaction 5), produces a hydroxycyclohexadienyl adduct (compound **B**). This adduct can undergo (acid-catalyzed) elimination of H_2O (reaction 4) to produce a radical cation (compound **E**). Short-lived intermediates of PAMSS ($\lesssim 1$ ms) are indicated in color. The aim of this study is to determine whether Ce^{3+} is a competitive repair agent for the radical cation (reaction 11), in terms of side reactions (reaction 7, 8 and 12–14).

The antioxidant properties of CNPs are dependent, also, on the ability to undergo redox cycling between the valences Ce^{3+} and Ce^{4+} ions (as $CeO_{2-\delta}$) on the surface of CeO_2 or Ce_2O_3 CNPs in aqueous solution.[11] Radical scavenging by Ce^{3+} is very effective in PFSA membranes, because the lifetime of HO$^\bullet$ is on the order of microseconds, thus with a relatively small concentration of Ce^{3+} of ~ 0.1 M over 90% of HO$^\bullet$ are quenched.[5] The ratio of Ce^{4+} to Ce^{3+} is influenced by the chemistry of the medium. For example, H_2O_2 and $HO_2^\bullet$, which are also present in a fuel cell membrane,[12] can reduce Ce^{4+} to Ce^{3+}:[13]

$$Ce^{4+} + H_2O_2 \rightarrow Ce^{3+} + HO_2^\bullet + H^+ \quad (k_2 = 1 \times 10^6 \ M^{-1} \ s^{-1}\ {}^{8,14})$$
(2)

$$Ce^{4+} + HO_2^\bullet \rightarrow Ce^{3+} + O_2 + H^+ \quad (k_3 = 2.7 \times 10^6 \ M^{-1} \ s^{-1}\ {}^{14})$$
(3)

Because the Ce^{4+} that is formed reacts with H_2O_2 and HOO$^\bullet$, the scavenger Ce^{3+} can effectively be restored. Thus, these

regenerative reactions enable a more effective catalytic HO$^\bullet$ scavenging mechanism by Ce^{3+}. In polyaromatic fuel cell membranes, however, owing to the very fast reaction with the aromatic units, the lifetime of HO$^\bullet$ is in the nanosecond range, thus around 3 orders of magnitude shorter than in PFSA membranes. Therefore, protecting polyaromatic polymers by scavenging of HO$^\bullet$ alone is not sufficient.[6] Nevertheless, we might exploit the redox cycling mechanism of Ce that forms the basis of its medicinal properties: we propose to use the Ce^{3+}/Ce^{4+} redox couple to 'repair' the damage to polyarylene type ionomers caused by attack of the OH$^\bullet$ radical. The question in this context is, given the chemistry of the polymer: does an intermediate exist that is sufficiently long-lived to be amenable to repair?

An intermediate formed as a result of OH$^\bullet$ attack on arylenes is the aromatic radical cation (Ar$^{\bullet+}$) (compound **E**, Fig. 1), produced by acid-catalyzed elimination of H_2O (reaction 9, Fig. 1) from the OH-adduct (compound **B**, Fig. 1).[15,16] Since proton exchange membrane fuel cells operate under acidic

conditions, elimination of H_2O is usually fast.[15–17] The redox potential $E°$ of Ce^{4+}/Ce^{3+} of 1.44 V[18] is favorable as compared to $E°(Ar^{•+}/Ar)$ = 2.0–2.4 V.[19] In previous work using poly-(α-methylstyrene sulfonate) (PAMSS) oligomers as model aromatic compound, we found that the lifetime of the radical cation increases with the degree of polymerization, potentially due to π–π interactions, and does not produce benzyl radicals due to the presence of the α-methyl group.[20] PAMSS is well soluble in water making it a viable candidate to study the kinetics of its reaction with Ce^{3+} in aquo. PAMSS represents a constituent of a fuel cell membrane. Though other model compounds representing polyarylene type polymers (e.g. polysulfones) are conceivable, they are beyond the current scope.

In the work reported here, we studied the interaction (reaction 11, Fig. 1) between Ce^{3+} and the aromatic radical cation of PAMSS (compound **E**) to investigate whether cerium could function as a regenerative antioxidant for repairing aryl-type polymers. To determine whether the repair pathway is viable we compared the regeneration kinetics with a potential side reaction, prominently, the reaction of the HO-adduct (compound **B**) with O_2 (reactions 7/−7 and 8, Fig. 1). The degree of polymerization of PAMSS was varied from 1 to 1700 in order to study the effect of $Ar^{•+}$ lifetime and redox properties. The results of this study are of high relevance to material scientists and engineers looking to improve the durability of hydrocarbon based fuel cell membranes, as well as for medicinists aiming to elucidate and optimize antioxidant mechanisms.

Materials and methods

PAMSS oligomers/polymers (>95% sulfonation degrees) with molecular weights M_w of 2660, 14 600, 73 800 and 354 000 Da, and polydispersity indices of <1.5, <1.2, <1.2 and <1.2, respectively, were supplied by PSS (Polymer Standards Service, Mainz, Germany). A 'monomeric unit' of PAMSS, 4-tert-butyl-benzenesulfonate, was used to represent a 'degree of polymeri-zation' of 1. Ce^{3+} was added as a salt, $Ce_2(SO_4)_3$, obtained from Sigma-Aldrich (≥99.99% purity). Water from a Millipore-Q system was used to prepare solutions that were saturated with O_2, N_2O, or Ar depending on the reaction studied. Samples were gas saturated in Schlenk-tubes which were repeatedly evacuated to 10 mbar and refilled (a minimum of 3 repeats) with the desired gas. The solutions were transferred from a gas-tight syringe (10 ml, Hamilton, SampleLock, Bonaduz, Switzerland) to the measurement cell via a syringe pump. Acidic pH was adjusted with H_2SO_4 (95-97% purity), while solutions at pH 7 were buffered with 0.1 mM phosphate buffer ($NaH_2PO_4\cdot H_2O$, >99% purity), unless stated otherwise. Experiments were carried out at room temperature (25 °C). tert-Butanol was obtained from Merck (Darmstadt, Germany) to scavenge $OH^•$ when needed.
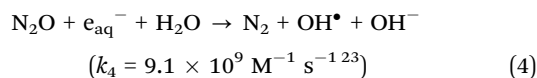
Pulse radiolysis

Pulse radiolysis experiments were carried out using a Febetron 705 (Titan Systems Corp., presently L-3 Communications, San Leandro, CA, USA), equipped with an optical detection system. For details see Nauser et al. (2008).[21] Irradiations were performed in a 6 cm quartz cell (Hellma, Müllheim, Germany) with <50 ns pulses of 2 MeV electrons. The dose was measured using a thiocyanate dosimeter.

Production of $OH^•$ radicals

Pulse irradiation of water results in the formation of primary species with yields $G(OH^•)$ (primary yield (molecules per 100 eV), pH 7), $G(e_{aq}^-)$ and $G(H^•)$ of 2.7, 2.65 and 0.6,[22–24] respectively, whereby G = 1 equals to 0.1036 µmol of a species generated species per 1 J kg^{-1} absorbed energy. The solutions were saturated with N_2O (22 mM) to increase the $OH^•$ yield and reduce side reactions. The solvated electron, e_{aq}^-, reacts with N_2O to yield additional $OH^•$:

$$N_2O + e_{aq}^- + H_2O \rightarrow N_2 + OH^• + OH^-$$
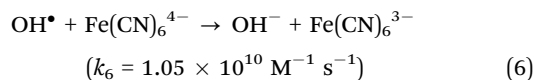$$(k_4 = 9.1 \times 10^9 \text{ M}^{-1} \text{ s}^{-1\ 23}) \qquad (4)$$

Reaction of $OH^•$ with PAMSS

Reaction of $OH^•$ with an aromatic unit (Fig. 1, reaction 5) produces a hydroxycyclohexadienyl adduct (Fig. 1, compound **B**).[20,25] Here, we quantified the rate constants for the reaction between the polymers and $OH^•$:

$$OH^• + PAMSS \rightarrow PAMSS(-OH)^• \quad (k_5) \qquad (5)$$

PAMSS radicals have relatively low extinction coefficients and side-reactions might be involved at high concentrations of radicals. To bypass and minimize this, we studied the reaction with $OH^•$ via competition with $Fe(CN)_6^{4-}$:

$$OH^• + Fe(CN)_6^{4-} \rightarrow OH^- + Fe(CN)_6^{3-}$$
$$(k_6 = 1.05 \times 10^{10} \text{ M}^{-1} \text{ s}^{-1}) \qquad (6)$$

At relatively low dose (~10 Gy), the concentration of $Fe(CN)_6^{4-}$ was ~50 µM and the concentration of PAMSS was varied. Under N_2O saturated conditions the radiation chemical yield (G) of $OH^•$ is ~5.6 × 10^{-7} mol J^{-1} and is unaffected by the PAMSS concentration (dilute solutions, ≤100 µM). Thereby, the absorbance at 420 nm ($Fe(CN)_6^{3-}$, ε_{420} = 1040 M^{-1} cm^{-1}) is solely affected by the PAMSS concentration via competition for $OH^•$. The absorption at 420 nm, virtually constant after ~5 µs, was measured.

Control experiments were performed using different dose/$Fe(CN)_6^{4-}$ ratios, as well as direct observation (details in the ESI†).

Reaction of hydroxycyclohexadienyl radicals with oxygen

Reaction of O_2 with hydroxycyclohexadienyl radicals (Fig. 1, reaction 7) produces an Ar–OH(–O_2) radical adduct (Fig. 1, compound **C**):

$$PAMSS(-OH)^• + O_2 \rightleftharpoons PAMSS(-OH)(-O_2)^• \quad (k_7/k_{-7}) \qquad (7)$$

The addition of O_2 to hydroxycyclohexadienyl radicals was studied by varying the O_2 concentration, and observing the

4518 | Phys. Chem. Chem. Phys., 2020, 22, 4516–4525

This journal is © the Owner Societies 2020
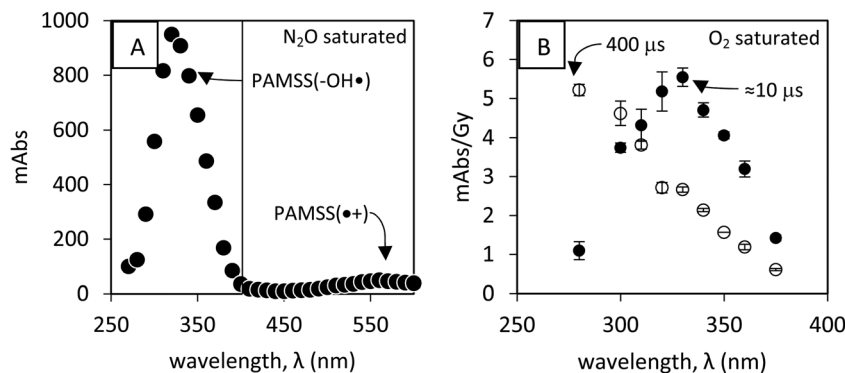
Fig. 2 (A) Spectrum of 5 µM poly(α-methylstyrene sulfonate) M_w = 354 000 Da. Dose ∼15 Gy, N_2O saturated, pH ∼ 7. The absorption was highest within the time interval of the first 10 µs after the pulse. (B) Spectrum of 32.7 µM poly(α-methylstyrene sulfonate) M_w = 14 600 Da. Dose ∼50 Gy, O_2 saturated (1.25 mM), pH ∼ 7. Highest within 10 µs (filled symbols, see Fig. S8-1A, ESI†) and 400 µs (open symbols) after the pulse. Absorbances <280 nm are omitted because optimization of spectral resolution at the expense of incident light intensity resulted in noisy and inaccurate absorbance.

effect on the kinetic trace of hydroxycyclohexadienyl radicals. Mixtures of N_2O/O_2 were used and the concentration of O_2 in the samples was determined *via* the partial pressure of O_2 and its solubility in water (1.25 mM at 1.0 atm). O_2 concentrations ranged from 0 to 1.25 mM. Doses applied were ∼40 Gy. All experiments reported were reproduced at least five times.

The characteristic λ_{max} for hydroxycyclohexadienyl-type radicals is ∼325 nm, Fig. 2. However, other species, among which the Ar–OH(–O$_2$) radical adduct, absorbs also in this spectral range (Fig. 2B). Moreover, the addition of oxygen is reversible[25] with an equilibrium constant K on the order of $\geq 10^3$ M^{-1},[25] because the reverse reaction is relatively slow (reaction −7, Fig. 1, with k_{-7} = 4.5($\pm$0.9) × 10^3 s^{-1} as an upper limit for poly(styrene sulfonate) (PSS)[26]).

The addition reaction was monitored at λ = 360 nm, chosen empirically such that both the relative absorption of the OH$^{\bullet}$-adduct (relative to the Ar–OH(–O$_2$) adduct) and absolute absorption are maximized (Fig. S4B, ESI†). Based on earlier results[25,26] we identified the decay within ∼10–20 µs of the absorption maximum. The kinetic traces were fitted with pseudo-first order functions. This analytical setup minimized the need of fitting to equilibria or taking into account side reactions, such as $^{\bullet}$OOH elimination (reaction 8, Fig. 1, with k_8 = 2.7($\pm$0.3) × 10^3 s^{-1} for PSS[18]) to form a stable hydroxylated product (compound **D**). Thus, we can fit kinetic traces for the OH$^{\bullet}$-adduct with minimal interference.[25]
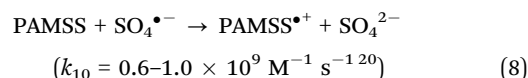
Control experiments were performed using gas mixtures of Argon/O$_2$ and N_2O/O_2 under low doses (∼10 Gy) to characterize the relevance of the yield of OH-adducts (details in Fig. S8, ESI†) on the apparent rate constants.

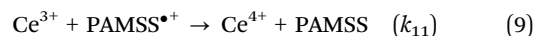**Production of radical cations and reaction with Ce^{3+}**

Under N_2O/O_2 conditions and pH ∼7 the yield of radical cations from OH$^{\bullet}$-adducts (*e.g. via* reaction 9, Fig. 1) is low: 0.1–1 µM for M_w = 354 000 (Fig. 2A, $\lambda_{max} \cong 560$ nm), and below our detection limit for smaller polymer weights. When the radical cation was produced at pH ∼7 *via* elimination from the PAMSS-OH$^{\bullet}$ adduct (M_w = 354 000 Da), no reaction between the radical cation and Ce^{3+} was observed.

Rate constants for the elimination of OH^{-}/H_2O have previously been identified as ∼10^4 s^{-1} for a range of aryl-type OH$^{\bullet}$-adducts,[16] whereas for the reaction between radical cation and H_2O (reaction −9, Fig. 1) values differ 10^1–10^7 [16] (k_{-9} = 1–2 × 10^4 s^{-1}, Fig. 5 and Fig. S10–S12, ESI†). Thus, simultaneous production of radical cations *via* elimination (reaction 9, Fig. 1) from the PAMSS-OH$^{\bullet}$ adduct (Fig. 2A) might obscure the depletion *via* reaction with Ce^{3+} (reaction 11, Fig. 1).

Bypassing the H_2O/OH^{-} elimination from PAMSS-OH$^{\bullet}$ route, radical cations were produced by electron transfer to sulfate radicals (reaction 10, Fig. 1):

$$PAMSS + SO_4^{\bullet -} \rightarrow PAMSS^{\bullet +} + SO_4^{2-}$$

$$(k_{10} = 0.6\text{–}1.0 \times 10^9 \text{ M}^{-1} \text{ s}^{-1}\ {}^{20}) \qquad (8)$$

Potassium peroxodisulfatesulfate (50 mM) was added to argon-saturated solutions at pH ∼ 2 (adjusted with H_2SO_4). Dose was ∼100 Gy, and *t*BuOH (100 mM) was added to scavenge the primary OH$^{\bullet}$ radicals. Concentrations of PAMSS were used according to the degree of polymerization (*e.g.* 4.5 mM for PAMSS-354 000). We varied the Ce^{3+} concentration to obtain pseudo first-order rate constants for the reaction:

$$Ce^{3+} + PAMSS^{\bullet +} \rightarrow Ce^{4+} + PAMSS \quad (k_{11}) \qquad (9)$$

Results and discussion

Reaction of OH$^{\bullet}$ with PAMSS

The introduction of PAMSS to a solution containing Fe(CN)$_6^{3-}$ led to a decrease in the absorption recorded at 420 nm (*i.e.* reaction between Fe(CN)$_6^{3-}$ and OH$^{\bullet}$). This is indicative of a reaction between OH$^{\bullet}$ and PAMSS (*i.e.* a competition for OH$^{\bullet}$). Taking into account reaction 6 (Fig. 1, Fe(CN)$_6^{3-}$ + OH$^{\bullet}$) we fitted the data (blue lines and triangles in Fig. 3) to obtain k_5 = 5.7($\pm$0.2) × 10^{11} M^{-1} s^{-1} for the bimolecular reaction rate constant between PAMSS-354 000 (the polymer with the highest M_w) and OH$^{\bullet}$ (Fig. 1, reaction 5). By extension, we obtained the following data for the series of oligomers/polymers with different molecular weight, given in Table 1.
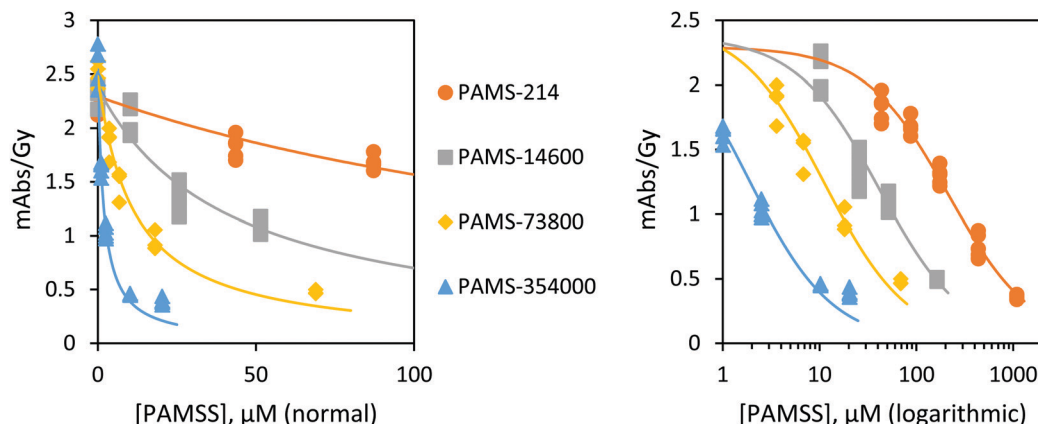
This journal is © the Owner Societies 2020

Phys. Chem. Chem. Phys., 2020, **22**, 4516–4525 | **4519**

Fig. 3 The determination of the reaction rate constant between PAMSS and OH$^\bullet$ via competition with Fe(CN)$_6^{3-}$. The Fe(CN)$_6^{3-}$ concentration was approximately 100 μM. Dose $\sim$25 Gy. Lines denote fitting based on competition kinetics.

Table 1 Rate constants for the reaction between OH$^\bullet$ and PAMSS polymers/oligomers (c.k. = competition kinetics)

Polydispersity index	Molecular weight, M_w (Da)	k_5 (M^{-1} s^{-1})	k_5/n^d	Source
1	214[a]	4.9($\pm$0.1) × 10$^{9\,b}$	4.9($\pm$0.1) × 10^9	This work, c.k.
<1.5	2660	1.3($\pm$0.2) × 10$^{10\,b}$	9.4 × 10^8	This work, c.k.
n/a	2640	2.0 × 10^{10}	1.5 × 10^9	Dockheer et al.[c 20]
n/a	6400	2.5($\pm$0.5) × 10^{10}	7.7 × 10^8	Dockheer et al.[c 20]
<1.2	14 600	2.8($\pm$0.2) × 10$^{10\,b}$	3.8 × 10^8	This work, c.k.
<1.2	73 800	9.4($\pm$0.3) × 10$^{10\,b}$	2.5 × 10^8	This work, c.k.
<1.2	354 000	5.7($\pm$0.2) × 10$^{11\,b}$	3.2 × 10^8	This work, c.k.
<1.2	354 000	5.8($\pm$0.3) × 10^{11}	3.2 × 10^8	This work, direct obs.

[a] 4-tert-Butyl-benzenesulfonate. [b] Using a Fe(CN)$_6^{3-}$: OH$^\bullet$ ratio of $\geq$5 : 1. Controls using ratios of >10 : 1 gave 3.1($\pm$0.2) × 10^{10} M^{-1} s^{-1} for PAMSS-14 600 and 6.9($\pm$0.9) × 10^{11} M^{-1} s^{-1} for PAMSS-354 000. [c] Dockheer et al. evaluated the kinetics via direct observation of the OH-adduct. [d] Whereby n was taken as the ratio between the molecular weights (M_w) between the polymer and monomer.

The apparent yield of adducts (absorption at 360 nm) under N$_2$O atmosphere is less than twice that obtained under O$_2$ (3.2 and 5.9 abs Gy^{-1}, resp.), i.e. G(N$_2$O)/G(O$_2$)= 1.86 $\pm$ 0.04 (Fig. 4A). The ratio in yields of the primary radicals, G(OH$^\bullet$, N$_2$O) + G(H$^\bullet$, N$_2$O) = 0.622 and G(OH$^\bullet$, O$_2$) + G(H$^\bullet$, O$_2$) = 0.342, i.e. G(N$_2$O)/G(O$_2$) = 1.82, is similar. We infer that the absorption corresponds to 5–10% PAMSS-H$^\bullet$ adducts. Nevertheless, measurement of k_5 via direct observation produced the same value as obtained via competition kinetics (Table 1), Fig. S1 (ESI†). The suite of control studies indicated the stability of the method (Table 1).

We obtained larger values for k_5 for larger molecular weights. However, when we express k_5 per monomer unit, there is a notable decrease. The data match earlier observations by, e.g., Dockheer et al.[20] for a more limited range of M_w (Table 1); we find our values either slightly lower or equal to what has been reported.

The influence of size could be expressed as $k_5 \sim [n]^{0.60\pm0.08}$ ($k_5 \sim [n]^{0.57}$ including Dockheer et al. data,[20] Fig. 6), wherein $[n]$ is the degree of polymerization. Variation in the polydispersity index (PDI) between the polymers is not expected to influence the relationships obtained in this study (since PDI < 1.2). The "reaction exponent", here 0.60 $\pm$ 0.08, is sometimes defined as θ:[27,28]

$$\theta = \frac{(3+g)}{z} \qquad (10)$$

In case the polymer dynamics are 'Rouse-like' (single un-entangled chain; no significant interactions between chain segments) z = 4. In turn, g = 0 represents a non-interacting electron–electron system (the correlation hole[29] is screened out). Then, the reaction exponent is $(3 + 0)/4 = 0.75$. Indeed, k_5 values are near the "diffusion control": $k_5 \sim [n]^{0.60}$, i.e. $0.60 \pm 0.08 \lesssim 0.75$. Thus, k_r is largely independent of the reactivity of the reaction site.

Decay of hydroxycyclohexadienyl radicals

The first order decay of PAMSS-OH$^\bullet$ seems to be a function of the yield of OH$^\bullet$-adducts (Fig. S3 and S8, ESI†). If we assume the yield of OH$^\bullet$-adducts is 8 times larger under 40 Gy and N$_2$O, as compared to under 10 Gy and argon, we derive based on Fig. S3 and S8 (ESI†) a slope (rate constant) on the order of $5(\pm1) \times 10^2$ M^{-1} s^{-1} (Fig. S3, ESI†). The intercept is $2.2(\pm0.5) \times 10^3$ s^{-1} (Fig. S3, ESI†). The half-life of the PAMSS-OH$^\bullet$ adduct (as observable at $\sim$325 nm) generally increased with M_w (e.g. $k_{obs} = 1.4(\pm0.3) \times 10^4$ s^{-1} and $6.1(\pm0.3) \times 10^3$ s^{-1} for M_w = 2660 and 14 600, resp.), though quantification requires the relative (effective) concentration of OH-adducts for different M_w. PAMSS-OH adducts seem to be more stable as the M_w increases.

A neighboring monomer might interact with the radical site in such a way that its intrinsic reactivity is lowered, or the
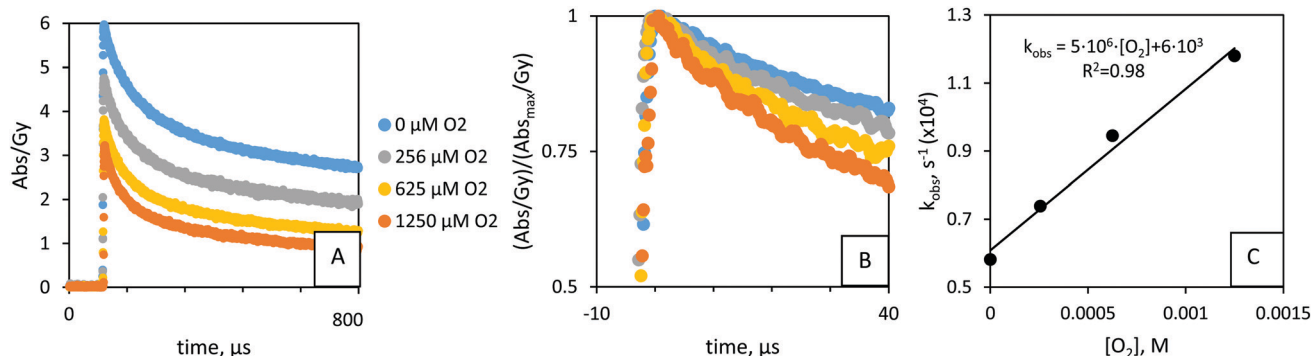
4520 | Phys. Chem. Chem. Phys., 2020, **22**, 4516–4525

This journal is © the Owner Societies 2020

Fig. 4 (A) Kinetic traces for the reaction between (decay of) PAMSS-14 600($-$OH$^\bullet$) adduct and O$_2$, monitored at 360 nm. Time-averaged. 32.7 μM PAMSS-14 600, $\sim$25 °C. pH $\sim$ 7; 5 replicates per data point. Colors show the concentration of O$_2$ in μM. (A) N$_2$O/O$_2$ solutions., $\sim$40 Gy. Long time interval. (B) N$_2$O/O$_2$ solutions. $\sim$40 Gy. Short time interval; normalized by the absorption at t_0 ($\sim$2 μs). (C) N$_2$O/O$_2$ solutions. $\sim$40 Gy. Pseudo 1st order rate constants *versus* O$_2$ concentration. k_7 = 4.8($\pm$0.4) $\times$ 10^6 M^{-1} s^{-1}.

coiling of the polymer chain may decrease its accessibility. Values for propagation in radical polymerisations are typically $10^{3\pm1}$ M^{-1} s^{-1},[30] *i.e.* slow due to steric crowding about the radical center. Based on this, we consider the value 5($\pm$1) $\times$ 10^2 M^{-1} s^{-1} to correspond to reaction 12 (crosslinking and/or disproportionation, k_{12}) in Fig. 1.

Protonation of OH$^\bullet$-adducts occurs with a rate constant of k = 1–2 $\times$ 10^9 M^{-1} s^{-1}[16] implying a pseudo 1st order rate constant of 1–2 $\times$ 10^2 s^{-1} at pH 7, whereas the elimination of OH$^-$ occurs with a rate on the order $\sim$10^4 s^{-1} for a range of aryl-type OH$^\bullet$-adduct monomers.[16] Thus, the value of 2.2($\pm$0.5) $\times$ 10^3 s^{-1} might characterize reaction 9 (either elimination of OH$^-$ or acid-catalysed elimination of H$_2$O, k_9) of PAMSS-14 600($-$OH$^\bullet$) as denoted in Fig. 1, reaction 9/$-$9.

Reaction of hydroxycyclohexadienyl radicals with oxygen

Upon exposure of the hydroxycyclohexadienyl radicals to O$_2$ we observed a shift to shorter wavelengths over time (Fig. 2B). $\sim$400 μs after the pulse, there was no apparent contribution from the OH-adduct (as seen at λ_{max} = 325 nm) to the absorbance anymore (Fig. 2B, see also ESI†). The shift to shorter wavelength for reaction products under O$_2$ atmosphere (Fig. 2B and Fig. S4–S6, ESI†) has been observed in related studies[20,25] and is attributed to O$_2$-radical adducts.

The yield of OH$^\bullet$-adducts varied for different ratios of N$_2$O/O$_2$ and between pulses (Fig. 4A); the concentration of OH$^\bullet$-adducts under N$_2$O/O$_2$ mixtures was directly proportional to the yield of OH$^\bullet$, see Fig. 4A and Fig. S7 (ESI†). This was taken into account when evaluating the pseudo-first order reaction with O$_2$ (reaction 7, Fig. 1):[24] we consider the relative concentrations of OH$^\bullet$-adducts. Thus, Fig. 4A was corrected for the adduct yields (maximum absorbance, at $\sim$2 μs), to give Fig. 4B.

Control studies indicated the stability of the method (Fig. S8, ESI†): H$^\bullet$ is quenched by PAMSS, rather than O$_2$. There is no difference between the k_7 values obtained from series under argon or N$_2$O. Therefore, PAMSS-14 600($-$H$^\bullet$) adducts react slower with O$_2$ than do PAMSS-14 600($-$OH$^\bullet$) adducts and do not contribute significantly to the result. Different initial yields of

PAMSS-14 600($-$OH$^\bullet$) adducts (at t = 2 μs), do not appear to affect the results (Fig. 4C and Fig. S8, ESI†). Thus, in the range of 2 μs to 10–20 μs, there is no measurable equilibration or elimination of OOH$^\bullet$ yet. Compared to 1.25 $\times$ 10^{-3} M for O$_2$ (in O$_2$ saturated solutions), the experimental series may also yield superoxide, O$_2^{\bullet-}$ (Fig. S8-1A, ESI†), in 10 μM (higher-end estimation). In O$_2$ saturated solutions ($\sim$1.25 mM) G(OH$^\bullet$) $\sim$ 2.8 $\times$ 10^{-7} mol J^{-1} and G(O$_2^{\bullet-}$) $\sim$ 3.4 $\times$ 10^{-7} mol J^{-1}. The reaction between PAMSS-OH and O$_2$ is thermodynamically favored (compared to that with O$_2^{\bullet-}$) based on the energies of their frontier orbitals:[31] $|E_{SOMO}(O_2) - E_{SOMO}(PAMSS\text{-}OH^\bullet)| < |E_{SOMO}(O_2^{\bullet-}) - E_{SOMO}(PAMSS\text{-}OH^\bullet)|$, *i.e.* $\Delta E \sim$ 0.4 eV $< \Delta E \sim$ 0.9 eV (in-house calculation[32–34]). The influence of O$_2^{\bullet-}$ has not been reported in related studies (under high O$_2$ concentrations[25]). Thus, the reaction between O$_2^{\bullet-}$ and PAMSS-OH is of minor importance, and the rate constants for addition of O$_2$ obtained in this study can be considered accurate.

From fitting we obtained a rate constant k_7 = 4.8($\pm$0.4) $\times$ 10^6 M^{-1} s^{-1} for the reaction between PAMSS-14 600($-$OH$^\bullet$) and O$_2$ (see ESI† for other M_w) in Fig. 4C. The reaction of a carbon-centered radical with O$_2$ to form the corresponding peroxyl radical generally proceeds with a rate constant on the order of 10^9 M^{-1} s^{-1}.[35] However, because of electron delocalization in allylic and dienylic C-centered radicals, oxygen binds relatively weakly, which results in slower and reversible O$_2$ addition. These notions are in agreement with the data obtained. Other factors explaining the relatively low rate constants include steric hindrance (*tert*-butyl) and polarity (sulfate) but need to be studied in more detail.

There appeared to be an influence of molecular weight, as a k_7 of 2.2($\pm$0.3) $\times$ 10^7 M^{-1} s^{-1} was found for the 4-*tert*-butyl-benzenesulfonate ($-$OH$^\bullet$) adduct. The data are in the same order as was found for PSS-1100($-$OH$^\bullet$): k = 3.0($\pm$0.5) $\times$ 10^7.[26] For the reaction between the OH$^\bullet$-adducts and O$_2$, k_7 scales with n: $k_7 \sim [n]^{-0.26\pm0.07}$. PSS data[26] might be included in the analysis if no significant influence by the extra methyl group is expected on the reaction thermochemistry, relative to the effect of M_w (Fig. 6). The influence of polymer size on the reaction between PAMSS($-$OH$^\bullet$) and O$_2$ ($-$0.26 $\pm$ 0.07) is different (2σ) from for the reaction between PAMSS and OH$^\bullet$ (0.60 $\pm$ 0.08).

This journal is © the Owner Societies 2020

Phys. Chem. Chem. Phys., 2020, **22**, 4516–4525 | **4521**

Since there is only 1 reactive site on the polymer, no relationship with n ($k_7 \sim [n]^0$) should be expected if diffusive or quantum-chemical effects are absent. Instead, the polymer dynamics *i.e.* diffusive pathway (z) and/or quantum-chemical properties (g) (eqn (10)) are affected (<0) by the breaking of aromaticity by OH$^\bullet$ to produce the hydroxycyclohexadienyl radical. It is worth noting that hydroxycyclohexadienyl radicals are relatively electron-rich and non-planar (Fig. 1, compound **B**), which would disfavor π–π interaction.

Decay of radical cations

In argon-saturated conditions and pH $\sim$ 2, SO$_4^{\bullet-}$ radicals were produced from the reaction between peroxodisulfate and the solvated electron. SO$_4^{\bullet-}$ radicals oxidize PAMSS to produce a radical cation observable at 560 nm. We detected radical cations for $2600 \geq M_w \geq 354\,000$, whereas for the 4-*tert*-butylbenzenesulfonate (*i.e.* the monomer unit) no radical cations could be observed. The half-life of the radical cation was found to be $\sim$40 to $\sim$100 µs depending on the chain length (Fig. 5). The influence of size was reported earlier by Dockheer *et al.* for a more limited range of M_w.[20]

The radical cations showed longer lifetimes upon increasing the molecular weight of the polymer (Fig. 6 and Fig. S10 and S11, ESI†), with reaction exponents ($k \sim [n]^{0.09\pm0.03}$) similar to those for the reaction between the radical cation and Ce^{3+}

(0.12 ± 0.01). Extrapolation of the data recorded in absence of O$_2$ (under Ar), using a power function in Fig. 6 results in $k = 1.6 \times 10^4$ s^{-1} for the first-order decay of the 4-*tert*-butylbenzenesulfonate radical cation ($\sim$40 µs half-life). This is relatively low compared to simple arenes, or even *tert*-butylbenzene cations (10^5–10^6 s^{-1} [16]). The mode of decay by the radical cations is uncertain. The α-methyl group prevents formation of a benzyl radical *via* a proton elimination (splitting) reaction and, instead, elimination of the sulfate was suggested[20] or dealkylation (scission), Fig. 1. The cation might react intramolecularly with a nearby monomer,[16] requiring a k of 10^6–10^7 s^{-1}. This is unlikely based on thermodynamic grounds, and it would likely result a shift in λ_{max} (for a similar radical cation), which was not observed. A radical–radical reaction would involve rate constants in the range of 10^8–10^9 M^{-1} s^{-1} (diffusion-limited, no thermodynamic arguments). This mechanism does not explain the size dependence observed and the decay that is still observed at very low concentrations, $\sim$$10^4$ s^{-1}. Rate constants for addition of H$_2$O to the radical cation (*i.e.* the backward reaction −9, Fig. 1) to form the water adduct are on the order of 10^2–10^3 M^{-1} s^{-1}.[16] The decay observed in acidic aqueous solution is given by $k = 6 \times 10^3$–6×10^4 s^{-1}. Addition of H$_2$O to the radical cation would occur *via* direction of the lone pair into the SOMO of the radical cation. The cation, and by extension the energy of this SOMO, could be subject to
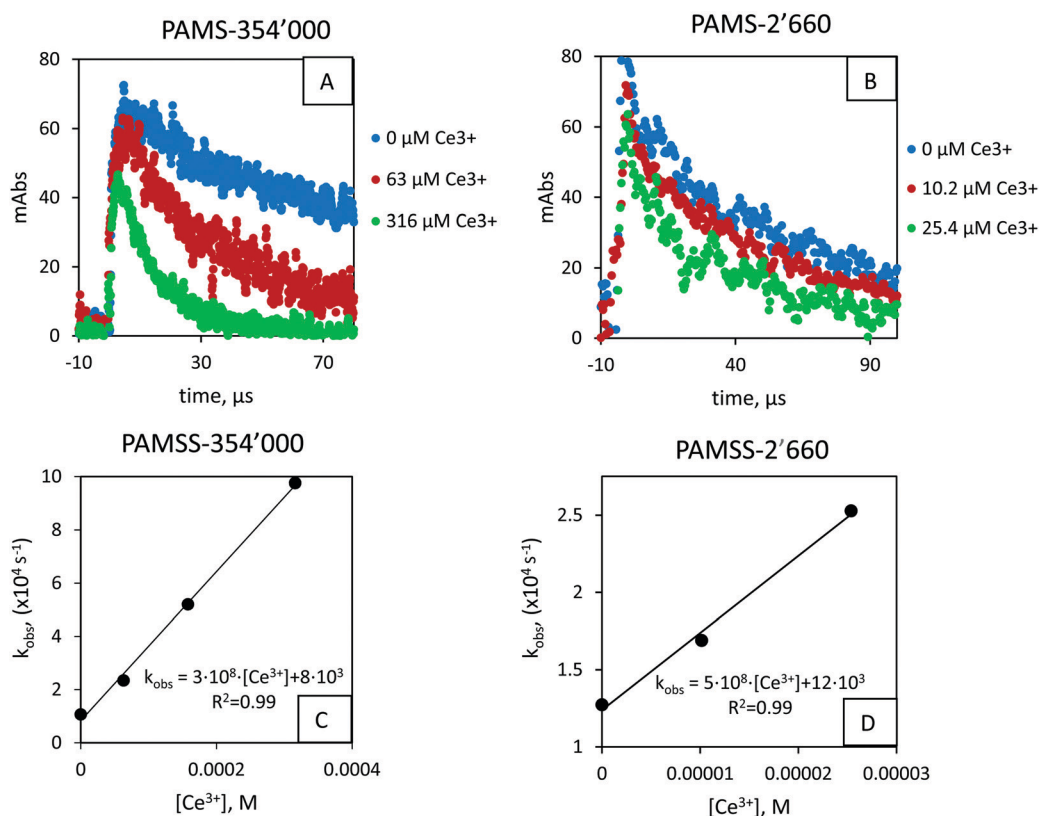

Fig. 5 (A and B) Kinetic traces for PAMSS-354 000 and PAMSS-2660, resp. for various Ce^{3+} concentrations. For visibility, only 3 kinetic traces are shown per graph. (C and D) Pseudo first-order rate constants *versus* Ce^{3+} concentration. $k_{11} = 2.8(\pm0.2) \times 10^8$ M^{-1} s^{-1} and $k_{11} = 5.0(\pm0.4) \times 10^8$ M^{-1} s^{-1} for PAMSS-354 000 and PAMSS-2660, resp. Data for $M_W = 14\,600$ and $M_W = 73\,800$ can be found in the ESI.†
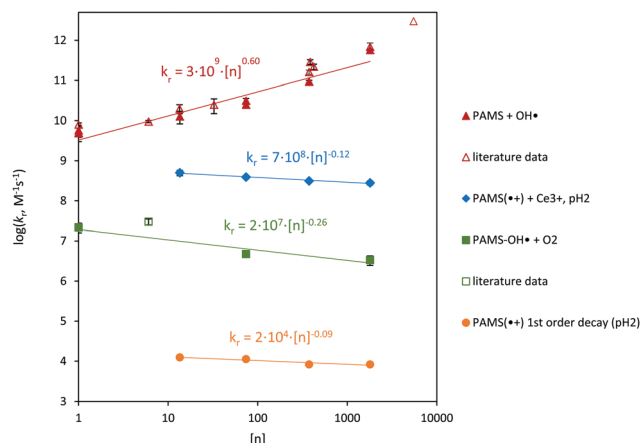
Fig. 6 Combined results for the reactions studied. Rate constants are plotted *versus* the degree of polymerisation, [n]. Literature data refer to Behar (1991),[37] Behar and Rabani (1988),[38] Bhardwaj *et al.* (2001)[39] and Dockheer *et al.* (2010)[26] for PSS and PAMSS, as well as control experiments. 'Reaction exponents': θ = 0.60 ± 0.08 for PAMSS + OH•, θ = −0.12 ± 0.01 for PAMSS•+ + Ce³⁺, θ = −0.26 ± 0.07 for PAMSS(−OH•) + O₂, and θ = −0.09 ± 0.02 for the first order decay of PAMSS•⁺.

intramolecular π–π interaction. As a result, the interaction can lower the rate of H₂O addition. Taking the molar concentration of H₂O for a dilute solution, k_{-9} would be 2(±1) × 10⁶ M⁻¹ s⁻¹.

Reaction of radical cations with Ce³⁺

Excluding the 4-*tert*-butylbenzenesulfonate (n = 1), the radical cations produced from the oligomers/polymers were exposed to Ce³⁺. For all molecular weights, a decrease in the lifetime of the radical cation was observed with increasing Ce³⁺ concentration. The influence of Ce³⁺ was attributed to the reduction of the radical cation back to the starting compound (reaction 11, Fig. 1). Minor bleaching was observed in some cases (Fig. S11A, ESI†), potentially due to reaction −1 (*cf.* Fig. 1). From the plot of pseudo-first order reaction rates *versus* concentration, reaction rate constants were obtained, *e.g.* for the PAMSS-14 600 radical cation in Fig. 5 we obtained k_{11} = 3.9(±0.2) × 10⁸ M⁻¹ s⁻¹ (see ESI† for other M_w).

As a validation exercise, experiments were conducted for a lower PAMSS (73 800) and higher persulfate concentrations, as well as under higher pH (Fig. S12, ESI†). The same value for k_{11} was obtained for the series when fitting the kinetic traces over a short time regime, indicating the stability of the method. Nevertheless, the observed rate constants are higher at pH ~ 3, as compared to pH ~ 2. An offset of 2.9(±0.2) × 10⁴ s⁻¹ between regressions for pH ~ 3 and pH ~ 2 was obtained. The offset is partially attributed to the acid–base equilibrium (reaction, 9/−9, Fig. 1) (see previous section).

The influence of molecular weight on the reaction between the PAMSS radical cation and Ce³⁺ was considered. The 'reaction exponent' is −0.12 ± 0.01, *i.e.* $k_{11} \sim [n]^{-0.12 \pm 0.01}$. The value is similar to that observed for the reaction between the radical cation and H₂O (previous section), −0.09 (Fig. 6). The negative values support the interpretation that the thermochemistry of the radical cation is affected intramolecularly. Intramolecular charge–radical

stabilization has already been confirmed on a fundamental level: chemical reactivity is controlled by radicals flanking the charged groups or by charged groups flanking the radicals.[36] For the radical cations, too, a significant stabilization is implied, which may be expressed as θ < 0, eqn (10). The radical cation is initially produced on the outer 'surface' of the polymer coil with a high degree of polymerization (diffusion limited). Quantum-chemical stabilization (g, eqn (10)) can be a π-donation into the outer-surface cation hole (*i.e.* the electron deficiency), effectively delocalizing (transferring) the cation hole to center of the polymer. It is conceivable that the polymer dynamics (z, eqn (10)) are also affected, for example, through bridging between polymer segments to facilitate radical stabilization.

Extrapolation of the data resulted in k_{11} = 6.4(±0.7) × 10⁸ M⁻¹ s⁻¹ for the reaction between 4-*tert*-butyl-benzenesulfonate radical cation and Ce³⁺ (Fig. 6). No literature data could be found for reactions of Ce³⁺ with aromatic radical cations. However, the ferrous ion (Fe²⁺) reacts with (reduces) the radical cation of anisole with a rate constant of k = 6 × 10⁸ M⁻¹ s⁻¹ (pH 1.0) and with pseudocumene and isodurene radical cations with k = 6(±1)10⁷ M⁻¹ s⁻¹ (pH 2.5–3.5).[16] These reactions are dependent on the ionic strength of the solution and, potentially, the polarity of the cation (Nolte *et al.*, in prep.).[32]

Conclusion

The reaction between PAMSSS and OH• borders the diffusion-limit, resulting in the formation of hydroxycyclohexadienyl, *i.e.* OH radical adducts, Ar(–OH•). These adducts can react with O₂, k_r = 3 × 10⁶⁻⁷ M⁻¹ s⁻¹, depending on the molecular weight, to produce O₂ adducts. Even though Ar(–OH•) reacts with O₂, the effectiveness of this reaction depends on the thermodynamic equilibrium of H₂O elimination/addition, which is a function of pH. Under acidic conditions, the OH-adduct eliminates H₂O to form a radical cation. The polymeric radical cation was shown to react with Ce³⁺ with rate constants of 3–5 × 10⁸ M⁻¹ s⁻¹ influenced by intramolecular stabilization, likely including radical–charge (π–π) interaction. Radical cations could not be observed for the monomeric compound (4-*tert*-butyl-benzenesulfonate), for which no intramolecular stabilization is possible, potentially also due to the fast backward reaction (H₂O addition). The competition between the reaction pathways involving Ce³⁺ (the repair reaction) or O₂ (as an indicator for irreversible damage) can be fine-tuned by modifying the size and structure of PAMSSS through its effect on both steric/clustering and redox properties, with the 'repair' reaction with Ce³⁺ generally being more efficient (compared to O₂) for shorter polymer chains.

The results of this study show that repair and stabilization of polymeric radicals can be achieved using cerium ions and neighboring groups *via* suitable thermochemical and kinetic interactions. This has ramifications for the design of durable arylene type fuel cell membranes and polymeric materials in general. The results also provide a basis for more fundamentally understanding the mechanisms behind conventional

antioxidants in medicine, such as ceria nanoparticles, and represent a starting point for improvement of additives that detoxify radicals or intermediates formed therefrom, *e.g.*, *via* damage transfer or repair pathways.

Conflicts of interest

The authors have no conflicts of interest to disclose.

Acknowledgements

References

1 L. Gubler, *et al.*, Prospects for Durable Hydrocarbon-Based Fuel Cell Membranes, *J. Electrochem. Soc.*, 2018, **165**(6), F3100–F3103.

2 M. Danilczuk, F. D. Coms and S. Schlick, Visualizing Chemical Reactions and Crossover Processes in a Fuel Cell Inserted in the ESR Resonator: Detection by Spin Trapping of Oxygen Radicals, Nafion-Derived Fragments, and Hydrogen and Deuterium Atoms, *J. Phys. Chem. B*, 2009, **113**, 8031–8042.

3 G. V. Buxton, *et al.*, Critical Review of rate constants for reactions of hydrated electrons, hydrogen atoms and hydroxyl radicals ($^\bullet$OH/$^\bullet$O$^-$) in Aqueous Solution, *J. Phys. Chem. Ref. Data*, 1988, **17**, 513–886.

4 T. M. Nolte and A. M. J. Ragas, A review of quantitative structure–property relationships for the fate of ionizable organic chemicals in water matrices and identification of knowledge gaps, *Environ. Sci.: Processes Impacts*, 2017, **19**(3), 221–246.

5 L. Gubler and W. H. Koppenol, Hydrocarbon Proton Exchange Membranes, in *The Chemistry of Membranes Used in Fuel Cells: Degradation and Stabilization*, ed. S. Schlick, John Wiley & Sons, 2018, pp. 107–138.

6 L. Gubler, T. Nolte and T. Nauser, Antioxidant Strategies for Hydrocarbon-Based Membranes, *ECS Trans.*, 2018, **86**(13), 369–379.

7 L. Rubio, *et al.*, Antioxidant and anti-genotoxic properties of cerium oxide nanoparticles in a pulmonary-like cell system, *Arch. Toxicol.*, 2016, **90**(2), 269–278.

8 F. D. Coms, H. Liu and J. E. Owejan, Mitigation of Perfluorosulfonic Acid Membrane Chemical Degradation Using Cerium and Manganese Ions, *ECS Trans.*, 2008, **16**(2), 1735–1747.

9 L. M. Kohan, J. Meesungnoen, S. Sanguanmith, R. Meesat and J. Jay-Gerin, Radiolysis of the ceric-cerous sulfate dosimeter at elevated temperatures: Monte Carlo simulations, *Recent Res. Dev. Phys. Chem.*, 2014, **11**, 15–27, (ISBN: 978-81-7895-608-4).

10 E. Collinson, F. S. Dainton and J. Kroh, The radiation chemistry of aqueous solutions II. Radical and molecular yields for tritium β-particles, *Proc. R. Soc. London, Ser. A*, 1962, **265**, 422.

11 A. Karakoti, *et al.*, Redox-active radical scavenging nanomaterials, *Chem. Soc. Rev.*, 2010, **39**(11), 4422–4432.

12 L. Gubler, S. M. Dockheer and W. H. Koppenol, Radical (HO$^\bullet$, H$^\bullet$ and HOO$^\bullet$) Formation and Ionomer Degradation in Polymer Electrolyte Fuel Cells, *J. Electrochem. Soc.*, 2011, **158**(7), B755–B769.

13 B. C. Nelson, *et al.*, Antioxidant Cerium Oxide Nanoparticles in Biology and Medicine, *Antioxidants*, 2016, **5**(2), 15.

14 B. H. J. Bielski, *et al.*, Reactivity of HO$_2^\bullet$/O$_2^{\bullet-}$ radicals in aqueous-solution, *J. Phys. Chem. Ref. Data*, 1985, **14**(4), 1041–1100.

15 P. Oneill, S. Steenken and D. Schultefrohlinde, Formation of Radical Cations of Methoxylated Benzenes by Reaction with Oh Radicals, Tl^{2+}, Ag^{2+}, and So^{4-} in Aqueous-Solution – an Optical and Conductometric Pulse-Radiolysis and Insitu Radiolysis Electron-Spin Resonance Study, *J. Phys. Chem.*, 1975, **79**(25), 2773–2779.

16 J. Holcman, Formation and reactions of radical cations of substituted benzenes in aqueous media. A pulse radiolysis study, Roskilde, Denmark: Risø National Laboratory. Risø-M, No. 1947, 1977.

17 S. Steenken and P. Neta, Transient phenoxyl radicals: Formation and properties in aqueous solutions, in *The Chemistry of Phenols*, ed. Z. Rappoport, John Wiley & Sons, 2003, p. 1115.

18 L. Gubler, Radiation Grafted Membranes for Polymer Electrolyte Fuel Cells, Departement Chemie und Angewandte Biowissenschaften, Eidgenössische Technische Hochschule, Zürich, 2016, DOI: 20.500.11850/190017.

19 M. Jonsson, *et al.*, Redox Chemistry of Substituted Benzenes – the One-Electron Reduction Potentials of Methoxy-Substituted Benzene Radical Cations, *J. Phys. Chem.*, 1993, **97**(43), 11278–11282.

20 S. M. Dockheer, L. Gubler and W. H. Koppenol, Reactions of the tetraoxidosulfate($^{\bullet-}$) and hydroxyl radicals with poly-(sodium alpha-methylstyrene sulfonate), *Phys. Chem. Chem. Phys.*, 2013, **15**(14), 4975–4983.

21 T. Nauser, *et al.*, Reversible Intramolecular Hydrogen Transfer between Cysteine Thiyl Radicals and Glycine and Alanine in Model Peptides: Absolute Rate Constants Derived from Pulse Radiolysis and Laser Flash Photolysis, *J. Phys. Chem. B*, 2008, **112**(47), 15034–15044.

22 R. H. Schuler, L. K. Patterson and E. Janata, Yield for the Scavenging of OH$^\bullet$ Radicals in the Radiolysis of N$_2$O-Saturated Aqueous-Solutions, *J. Phys. Chem.*, 1980, **84**(16), 2088–2089.

23 C. von Sonntag, *The Chemical Basis of Radiation Biology*, Taylor & Francis, London, 1987.

24 R. H. Schuler, A. L. Hartzell and B. Behar, Track Effects in Radiation-Chemistry – Concentration-Dependence for the Scavenging of OH$^\bullet$ by Ferrocyanide in N$_2$O-Saturated Aqueous-Solutions, *J. Phys. Chem.*, 1981, **85**(2), 192–199.

25 X. W. Fang, *et al.*, Reversibility in the Reaction of Cyclohexadienyl Radicals with Oxygen in Aqueous-Solution, *Chem. – Eur. J.*, 1995, **1**(7), 423–429.

4524 | *Phys. Chem. Chem. Phys.*, 2020, **22**, 4516–4525

This journal is © the Owner Societies 2020

26 S. M. Dockheer, *et al.*, Damage to fuel cell membranes. Reaction of HO• with an oligomer of poly(sodium styrene sulfonate) and subsequent reaction with O_2, *Phys. Chem. Chem. Phys.*, 2010, **12**(37), 11609–11616.

27 B. Oshaughnessy, Effect of Concentration on Reaction-Kinetics in Polymer-Solutions, *Macromolecules*, 1994, **27**(14), 3875–3884.

28 B. Friedman and B. Oshaughnessy, Kinetics of Intermolecular Reactions in Dilute Polymer-Solutions and Unentangled Melts, *Macromolecules*, 1993, **26**(21), 5726–5739.

29 J. des Cloizeaux, *J. Phys.*, 1980, **41**, 223–238.

30 K. Matyjaszewski, Typical features of radical polymerization, in *Controlled and living polymerizations: from mechanisms to applications*, ed. K. Matyjaszewski and A. H. E. Müller, Wiley-VCH, Weinheim, 2009, ch. 3.2, pp. 105–106.

31 G. Klopman, Chemical Reactivity and Concept of Charge- and Frontier-Controlled Reactions, *J. Am. Chem. Soc.*, 1968, **90**(2), 223–234.

32 T. M. Nolte, T. Nauser, L. Gubler and W. J. G. M. Peijnenburg, Thermochemical unification of molecular descriptors to predict radical hydrogen abstraction with low computational cost, *Phys. Chem. Chem. Phys.*, 2019, submitted.

33 T. M. Nolte and W. J. G. M. Peijnenburg, Aqueous-phase photooxygenation of enes, amines, sulfides and polycyclic aromatics by singlet (a1Δg) oxygen: prediction of rate constants using orbital energies, substituent factors and quantitative structure–property relationships, *Environ. Chem.*, 2018, **14**(7), 442–450.

34 J. J. P. Stewart, *MOPAC*, Stewart Computational Chemistry, Colorado Springs, CO, USA, 2016.

35 D. Minakata, *et al.*, Development of Linear Free Energy Relationships for Aqueous Phase Radical-Involved Chemical Reactions, *Environ. Sci. Technol.*, 2014, **48**(23), 13925–13932.

36 T. Mazur and B. A. Grzybowski, Theoretical basis for the stabilization of charges by radicals on electrified polymers, *Chem. Sci.*, 2017, **8**(3), 2025–2032.

37 D. Behar and B. Behar, Pulse-Radiolysis Studies of Amino-benzenesulfonates – Formation of Cation Radicals, *J. Phys. Chem.*, 1991, **95**(19), 7552–7556.

38 D. Behar and J. Rabani, Pulse-Radiolysis of Poly(Styrenesulfonate) in Aqueous-Solutions, *J. Phys. Chem.*, 1988, **92**(18), 5288–5292.

39 Y. K. Bhardwaj, *et al.*, Radiation effect on poly(p-sodium styrene sulphonate) of different degrees of polymerization in aqueous solution: pulse radiolysis and steady state study, *Radiat. Phys. Chem.*, 2001, **62**(2–3), 229–242.